

DESIGN OF OPTIMIZED CONTOURLET FILTERS FOR IMPROVED CODING GAIN

Tobias Gehrke*, Thomas Greiner

Pforzheim University, Pforzheim, Germany, tobias.gehrke@hs-pforzheim.de

ABSTRACT

The separable wavelet transform has limited directional sensitivity and is suboptimal for compression of textured images. A finer directional resolution and better coding results can be achieved by contourlet transform. So far, directional filters based on design criteria that are unspecific to image compression were used for contourlet transform. We propose directional filters that are optimized specifically for image coding. Thereto, a filter design method that is based on maximization of coding gain was developed. Directional filters were designed for all images of two standard test image databases and compared experimentally to standard filters. In most cases the newly designed filters performed better than standard filters.

Index Terms— Contourlets, image coding, filter design

1. INTRODUCTION

Image transform coding uses the fact that the coefficients of an appropriate transform can be coded more effectively than the original pixels, due to the transform's ability to decorrelate image information. In lossy compression, storage space is further reduced by discarding or approximating coefficients that contribute less to the visual appearance of an image. Frequently, the separable wavelet transform is used for this task, but its limited directional sensitivity restricts its performance for images with distinct textures. Multiple alternative transforms attempt to increase directional sensitivity [1]. Among them, the mildly redundant contourlet transform allows arbitrarily fine directional partitioning, while sharing frequency and spatial sensitivity with wavelets [2]. Its quality of directional partitioning, thereby its coding performance depend on the frequency characteristics of the underlying directional filters. Here, a novel method for the design of these filters is proposed. Its difference to existing methods is covered in section 2, while the method itself is detailed in section 4.

2. RELATED WORK

Contourlet transform combined with different quantization and entropy coding methods was occasionally used for im-

age compression, e. g. [3, 4]. Results indicate that contourlet transform is advantageous for highly textured images, while it does not beat wavelet transform for smooth images due to its redundancy. Therefore, contourlet transform becomes less advantageous in downsampled images. This led authors to construct hybrid transforms, which use the directionally sensitive contourlet transform on fine scale levels and the non-redundant wavelet transform on coarse scale levels [5].

All applications of contourlet transform to image coding either use so called Phoong-Kim-Vaidyanathan-Ansari (PKVA) filters [6] or biorthogonal Cohen-Daubechies-Feauveau (CDF) filters [7] in the directional filtering stage. These filters were designed for low-/high-pass filtering within the separable or quincunx wavelet transform respectively. To obtain the directional sensitivity needed for contourlet transform, the non-separable PKVA-filters are modulated towards a fan-shaped frequency characteristic, while the separable CDF-filters have to be transformed into two-dimensional filters by the McClellan transform before being modulated as well. Two additional directional filter designs for contourlet transform exist, but have found no application to image coding so far. One is a variant of PKVA-filters, obtained by applying the mapping mechanism of [6] to a Chebyshev approximation of ideal one-dimensional low-pass filters [8]. The second is a design method based on the criterion of directional vanishing moments instead of considering frequency characteristics [9].

Thus, so far only directional filters that were neither designed specifically for directional filtering nor for coding applications are used for contourlet based image compression. We explore the potential of directional filters that maximize coding gain, which is a measure that is directly related to the quality of a compressed image. Those design methods are known for separable wavelets [10] and for frequency-selective quincunx filter banks [11] but not for directional filter banks. Preliminary results indicated that filter design for contourlets based on optimized coding gain is beneficial [12].

3. CONTOURLET TRANSFORM

Contourlet transform is a two-step transform [2]. In a first step an image x with N pixels, each associated with a two dimensional position \mathbf{n} , is separated into its low-pass and high-pass parts x_0 and x_1 by a Laplacian pyramid. Afterwards, a directional filter bank is used to dissect the high-pass part x_1

*This work was funded by the State of Baden-Württemberg, Germany, Ministry of Science, Research and Arts within the scope of Cooperative Research Training Group.

into K channels, which represent different orientations within the image. Directional filtering is performed by filters F_i , $i = 0 \dots 3$, which show fan-shaped frequency characteristic. These filters let either horizontal or vertical edges pass. Filtering of oblique edges is achieved by downsampling $x'(\mathbf{n}) = x(\mathbf{Q}_\mu \mathbf{n})$ with quincunx downsampling operators

$$\mathbf{Q}_0 = \mathbf{Q}_1^\top = \begin{pmatrix} 1 & -1 \\ 1 & 1 \end{pmatrix}, \quad (1)$$

which cause rotation by 45° (\mathbf{Q}_0 to the right, \mathbf{Q}_1 to the left). The number of channels $K = 2^L$, i. e. the directional resolution, is determined by the number of levels L within the directional filter bank. Each level $l = 1 \dots L$ comprises fan shaped filter F_i and quincunx downsampling operators \mathbf{Q}_μ . Levels $l > 2$ additionally use resampling $x'(\mathbf{n}) = x(\mathbf{R}_\nu \mathbf{n})$ with shearing operators

$$\mathbf{R}_0 = \mathbf{R}_1^{-1} = \mathbf{R}_2^\top = \mathbf{R}_3^{-1\top} = \begin{pmatrix} 1 & 1 \\ 0 & 1 \end{pmatrix}. \quad (2)$$

The output of the directional filtering stage, i. e. contourlet coefficients y_k of each channel $k = 0 \dots K - 1$, are used to reconstruct the original image by reverting the filter bank operations of the analysis stage with synthesis filters E_i and upsampling

$$y'_k(\mathbf{n}) = \begin{cases} y_k(\mathbf{Q}_\mu^{-1} \mathbf{n}), & \mathbf{Q}_\mu^{-1} \mathbf{n} \in \mathbb{Z}^2 \\ 0, & \text{otherwise} \end{cases}. \quad (3)$$

If contourlet coefficients y_k are quantized before reconstruction, as in lossy compression, the reconstructed image \tilde{x} is an approximation of the original image x .

4. NEW APPROACH

To keep compressed image \tilde{x} as similar as possible to original image x , filters that minimize the reconstruction error $\|\tilde{x} - x\|$ shall be obtained by the filter design procedure described below. Thereto equivalent filters that account for the modifications of the image from x to \tilde{x} by the directional filter bank are derived in sections 4.1, 4.2, and 4.3. Based on these filters, the reconstruction error and its normalized variant can be estimated quantitatively as shown in sections 4.4 and 4.5.

4.1. Lifting Filters

To ensure invertibility of the filter bank without imposing additional constraints, a lifting framework is used. Analysis and synthesis filters F_i and E_i are factored into Λ lifting steps each comprising a prediction filter $P_{2\lambda}$ and an update filter $P_{2\lambda+1}$, $\lambda = 0 \dots \Lambda - 1$, which operate on polyphase components of the image [13]. The same lifting filters are used throughout all channels and levels of the directional filter bank. We further impose prediction-update-symmetry and separability in z-domain

$$P_{2\lambda+1}(z) = -1/2 P_{2\lambda}(z) = 1/2 p_\lambda(z_0) p_\lambda(z_1) \quad (4)$$

as well as a symmetric impulse response

$$p_\lambda(z) = \sum_{\zeta=0}^{Z-1} (-1)^{\zeta+1} p_{\lambda\zeta} z^{-(\zeta+1)} + (-1)^\zeta p_{\lambda\zeta} z^\zeta \quad (5)$$

upon the lifting filters. This approach creates filters that are structurally identical to the PKVA-filters [6]. The ΛZ independent lifting filter coefficients $p_{\lambda\zeta}$ are subjected to optimization by the filter design procedure.

4.2. Fan-Shaped Filters

Fan shaped filters F_i and E_i are obtained from lifting filters P by expansion of their transfer functions:

$$\begin{pmatrix} F_{00}(z) & F_{01}(z) \\ F_{10}(z) & F_{11}(z) \end{pmatrix} = \prod_{\lambda=0}^{\Lambda-1} \begin{pmatrix} 0 & 1 \\ 1 & P_{2\lambda+1}(z) \end{pmatrix} \begin{pmatrix} 1 & 0 \\ P_{2\lambda}(z) & 1 \end{pmatrix} \quad (6)$$

and taking

$$\begin{aligned} F_0(z) &= z_1 F_{00}(z^{\mathbf{Q}_0}) + F_{01}(z^{\mathbf{Q}_0}) & E_0(z) &= z_1^{-1} F_1(-z) \\ F_1(z) &= z_1 F_{10}(z^{\mathbf{Q}_0}) + F_{11}(z^{\mathbf{Q}_0}) & E_1(z) &= -z_1^{-1} F_0(-z) \\ F_2(z) &= z_0 F_{00}(z^{\mathbf{Q}_1}) + F_{01}(z^{\mathbf{Q}_1}) & E_2(z) &= z_0^{-1} F_1(-z) \\ F_3(z) &= z_0 F_{10}(z^{\mathbf{Q}_1}) + F_{11}(z^{\mathbf{Q}_1}) & E_3(z) &= -z_0^{-1} F_0(-z), \end{aligned} \quad (7)$$

where

$$z^{\mathbf{Q}} = \begin{pmatrix} z_0 \\ z_1 \end{pmatrix} \begin{pmatrix} Q_{00} & Q_{10} \\ Q_{01} & Q_{11} \end{pmatrix} = \begin{pmatrix} z_0^{Q_{00}} \cdot z_1^{Q_{10}} \\ z_0^{Q_{01}} \cdot z_1^{Q_{11}} \end{pmatrix}$$

accounts for upsampling in the z-domain [11].

4.3. Equivalent Filters

One can interchange the order of filtering and resampling such that two filters and two resampling operations can be combined into a single filter and a single resampling operation. By recursive repetition, it is possible to construct equivalent filters H_k and G_k that resemble the effect of all filters within one channel k .

In a two level, i. e. four direction, filter bank the equivalent filter for channel k combines the filters of the first stage with upsampled versions of the filters of the second stage:

$$\begin{aligned} H_0^{(2)}(z) &= F_1(z) F_2(z^{\mathbf{Q}_0}) & H_2^{(2)}(z) &= F_0(z) F_2(z^{\mathbf{Q}_0}) \\ H_1^{(2)}(z) &= F_1(z) F_3(z^{\mathbf{Q}_0}) & H_3^{(2)}(z) &= F_0(z) F_3(z^{\mathbf{Q}_0}). \end{aligned} \quad (8a)$$

For any level $l > 2$ the equivalent filter is given by the recursive definition

$$H_k^{(l)}(z) = H_{k'}^{(l-1)}(z) F_i(z^{\mathbf{S}_{k'}^{(l-1)} \mathbf{R}_\nu}), \quad (8b)$$

where $k' = \lfloor k/2 \rfloor$ is the index of equivalent filter $H_{k'}^{(l-1)}$, which summarizes all previous filters in the current branch.

The second multiplicand is the upsampled version of the fan shaped filter of level l , whose type (F_0, F_3 vertical-pass; F_1, F_2 horizontal-pass) is determined by index

$$i = \begin{cases} k \bmod 4, & k < 2^{l/2} \\ k \bmod 4 + 2, & k \geq 2^{l/2} \wedge k \bmod 4 < 2 \\ k \bmod 4 - 2, & k \geq 2^{l/2} \wedge k \bmod 4 \geq 2 \end{cases} \quad (9)$$

Upsampling occurs by a combination of the equivalent dilation matrix $\mathbf{S}_{k'}^{(l-1)}$ as given by (11) with the current shearing matrix \mathbf{R}_ν as specified by (2). The type of shearing matrix is selected by

$$\nu = \begin{cases} \lfloor (k \bmod 4)/2 \rfloor, & k < 2^{l/2} \\ \lfloor (k \bmod 4)/2 \rfloor + 2, & k \geq 2^{l/2} \end{cases} \quad (10)$$

Equivalent filters for synthesis are obtained by replacing $H_k^{(l)}(z)$ by $G_k^{(l)}(z)$ and $F_i(z)$ by $E_i(z)$ in (8).

Similarly, the downsampling and upsampling operations can each be combined into resampling with equivalent dilation matrices. For a two level filter bank this matrix combines the quincunx resampling matrices of levels $l = 1$ and $l = 2$:

$$\mathbf{S}_k^{(2)} = \mathbf{Q}_0 \mathbf{Q}_1, \quad (11a)$$

while for levels $l > 2$ an additional shearing matrix \mathbf{R}_ν must be taken into account:

$$\mathbf{S}_k^{(l)} = \mathbf{S}_{k'}^{(l-1)} \mathbf{R}_\nu \mathbf{Q}_\mu. \quad (11b)$$

The type of quincunx matrix is obtained from the index of the accompanying fan-shaped filter i by $\mu = \lfloor \frac{i}{2} \rfloor$.

4.4. Reconstruction Error

The complete filter bank is merged into one equivalent analysis filter $H_k = H_k^{(L)}$ and one equivalent synthesis filter $G_k = G_k^{(L)}$ per direction k by (8). This is used to link the reconstruction error $\|\tilde{x} - x\|$ to the filter coefficients $p_{\lambda\zeta}$.

Variances of the high-pass image x_1 and of the coefficients y_k are linked by the impulse responses h_k of the equivalent analysis filters within each channel k :

$$\sigma_{y_k}^2 = A_k \sigma_{x_1}^2 = \left(\sum_{\mathbf{m} \in \mathbb{Z}} \sum_{\mathbf{n} \in \mathbb{Z}} h_k(\mathbf{m}) h_k(\mathbf{n}) \frac{R(\mathbf{m} - \mathbf{n})}{R(\mathbf{0})} \right) \sigma_{x_1}^2. \quad (12)$$

Constant A_k accounts for second order statistics of high-pass image x_1 , given by its autocorrelation R , and the influence of analysis filtering.

During quantization, an error called quantization noise q_k is added to the coefficients y_k . It can be modelled approximately as white uncorrelated noise, whose variance is proportional to the variance of the coefficients y_k [14]:

$$\sigma_{q_k} = \epsilon 2^{-b_k} \sigma_{y_k}. \quad (13)$$

Constant ϵ accounts for the type of quantizer and b_k specifies the number of bits spent on the quantized signal \tilde{y}_k . The expectation of mean square reconstruction error is the weighted sum of the quantization noise over all channels:

$$D_{\text{CT}} = \frac{1}{N} \sum_{\mathbf{n} \in \mathbb{Z}^2} \mathbb{E} \left[(\tilde{x}_1(\mathbf{n}) - x_1(\mathbf{n}))^2 \right] = \sum_{k=0}^{K-1} B_k \sigma_{q_k}^2. \quad (14)$$

Quantization noise q_k is thus linked to the expectation of mean square reconstruction error by the impulse responses of the analysis filters g_k through weighting factor

$$B_k = \frac{1}{K} \sum_{\mathbf{n} \in \mathbb{Z}^2} g_k^2(\mathbf{n}). \quad (15)$$

4.5. Coding Gain

A normalized variant of the error between the original image x and its compressed counterpart \tilde{x} , called coding gain Γ , serves as an objective function of optimization.

According to (13), quantization noise depends on the number of bits b_k that have been allocated to channels k and the variance of contourlet coefficients σ_{y_k} . Those channels that have a greater variance should be allocated more bits than others. The optimum number of bits for channel k is

$$b_{k \text{ opt}} = b + \frac{1}{2} \log_2 \frac{K B_k \sigma_{y_k}^2}{\prod_{\kappa=0}^{K-1} (K B_\kappa \sigma_{y_\kappa}^2)^{1/\kappa}} \quad (16)$$

if an average number of bits b is specified [15].

Reconstruction error (14) under the assumption of optimal bit allocation (16) is obtained by combining the analysis filtering relation (12) with the quantization model (13):

$$D_{\text{CT opt}} = (\epsilon 2^{-b} \sigma_{x_1})^2 \prod_{k=0}^{K-1} (K A_k B_k)^{1/\kappa}. \quad (17)$$

The reconstruction error (17) is normalized by the error that would result from direct quantization of the image pixels $D_{\text{DQ}} = (\epsilon 2^{-b} \sigma_{x_1})^2$ to obtain the coding gain [14]

$$\Gamma = \frac{D_{\text{DQ}}}{D_{\text{CT opt}}} = \prod_{k=0}^{K-1} (K A_k B_k)^{-1/\kappa}. \quad (18)$$

4.6. Optimization

Coding gain Γ was linked to the coefficients of lifting filters $p_{\lambda\zeta}$ by the system model (15), (12), (8), and (7) as well as via lifting filter symmetries (4) and (5). We implemented these equations in the functional programming language of Wolfram Mathematica[®]. Maximization of coding gain by varying coefficients $p_{\lambda\zeta}$ is a nonlinear, non-convex optimization problem, which was solved numerically by a nonlinear conjugate gradient method using the optimization algorithm of Mathematica[®] version 8.0.1.0.

5. RESULTS

Optimized directional filter banks were designed individually for each of the 52 images consisting of all photos out of the “Miscellaneous” set of the University of Southern California SIPI test image database¹ and all photos of the “New Image Compression Test Set”². These images show a broad variety of themes and vary in size between 256×256 pixels and 7216×5412 pixels. Designed filter banks have $K = 8$ directional channels and consist of lifting filters with one lifting step, i. e. $\Lambda = 1$, each comprising $Z = 3$ independent filter coefficients. These filter coefficients were subject to optimization using the method expounded in section 4.

5.1. Convergence

To check whether optimization converges towards a global maximum, five different sets of pseudo-random numbers in the range $[-1, 1]$ were used as initial values for filter coefficient optimization in addition to the coefficients of standard PKVA-filters. All six optimization runs led to the same maximum for 43 images (83 %), while multiple local maximums are found in nine images (17 %). For these nine images the highest coding gain was always found with the standard filters as initial values.

5.2. Coding Performance

The coding performance of the optimized filter banks were compared to standard PKVA-filters. As an input to the directional filter banks the high-pass parts of the images, obtained by Laplacian pyramid filtering with Daubechies 9/7 filters, were used. The directional coefficients were approximated by uniform quantization before synthesis filtering. Figure 1a depicts mean and standard deviation alongside minimum and maximum of the difference in peak signal-to-noise ratio (PSNR) between approximated high-pass images using optimized filters and the standard filters as a function of entropy of the transform coefficients. The average performance gap between standard and optimized filters increase with higher bit rates, reaching 1 dB for 1.5 bits per pixel.

5.3. Coding Performance within a Hybrid Transform

We examined, whether the advantage of optimized directional filters also holds within a complete compression processing chain. The compression algorithm consisted of a three level hybrid contourlet/wavelet transform, scalar uniform quantization, and the arithmetic coder of MATLAB Communications System Toolbox™ R2013b. On the finest level, an eight direction contourlet transform with optimized or – for comparison – standard PKVA-filters were employed. Daubechies 9/7 filters were used on the coarser, i. e. wavelet, levels and for the Laplacian pyramid. Figure 1b shows that, on average, optimized

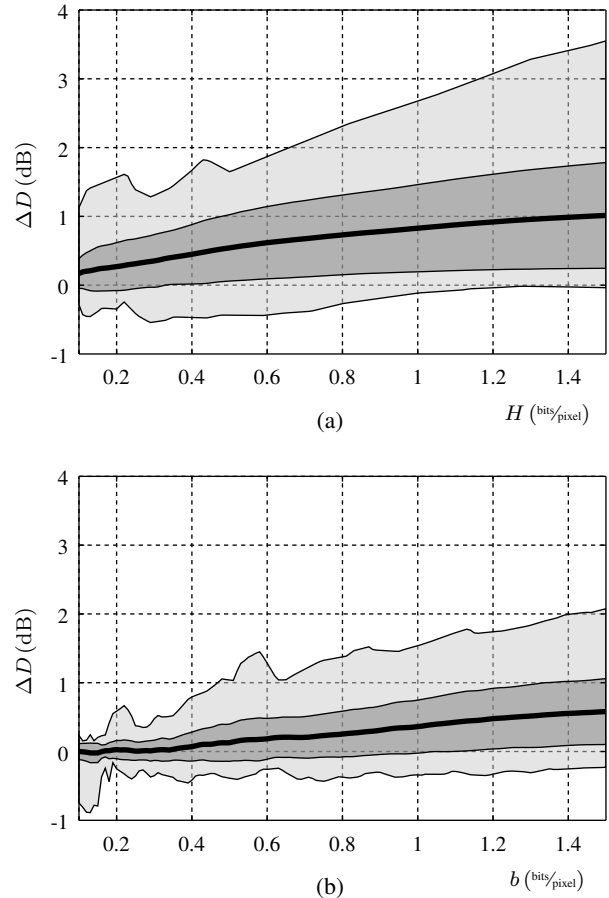


Fig. 1: Differences in image quality between transform with optimized directional filters and standard filters. Mean of results from 52 images (black line), according region bounded by standard deviation (dark grey area) and range (light grey area). (a) Difference in PSNR of approximated high-pass images as a function of entropy H of the transform coefficients. (b) Difference in PSNR of compressed images using hybrid transform as a function of bit rate b .

filters perform better than standard filters. The PSNR values for individual images at two exemplary bit rates are listed in Table 1. For a bit rate of 1.2 bits per pixel, 44 images (85 %) are better compressed with optimized filters than with standard directional filters, while for 0.2 bits per pixel the standard filters are outperformed by optimized filters in 31 cases (60 %).

6. CONCLUSION

A design method for directional filters used in contourlet transform was developed. The design is optimized for image coding through the use of maximum coding gain as the objective function. In most cases coding performance of the newly designed filters is better compared to standard directional filters. The study shows that directional filter design leaves room for optimization, which can be used e. g. by building filters adapted to specific classes of images.

¹<http://sipi.usc.edu/database/>

²http://www.imagecompression.info/test_images/

Image	PSNR (dB) 0.2 bits/pixel		PSNR (dB) 1.2 bits/pixel		Image	PSNR (dB) 0.2 bits/pixel		PSNR (dB) 1.2 bits/pixel		Image	PSNR (dB) 0.2 bits/pixel		PSNR (dB) 1.2 bits/pixel	
	Std	Opt	Std	Opt		Std	Opt	Std	Opt		Std	Opt	Std	Opt
4.1.01	30.42	30.33	38.69	38.95	5.1.12	27.48	27.48	37.88	37.84	big_building	30.90	30.89	40.48	41.13
4.1.02	30.06	30.05	38.70	38.76	5.1.14	25.06	25.05	32.76	32.82	big tree	35.34	35.32	41.72	42.60
4.1.03	34.63	34.66	43.77	43.93	5.2.08	26.85	26.84	35.74	35.63	boat.512	27.72	27.73	35.07	35.18
4.1.04	29.12	29.12	38.77	38.99	5.2.09	24.26	24.25	31.63	32.40	bridge	32.42	32.41	38.61	39.68
4.1.05	29.42	29.46	38.37	38.34	5.2.10	23.67	23.65	29.41	30.02	cathedral	34.63	34.57	42.02	42.90
4.1.06	23.58	23.57	31.00	31.07	5.3.01	28.85	28.87	36.11	36.39	deer	33.43	33.72	36.35	37.43
4.1.07	35.31	35.41	47.13	48.18	5.3.02	26.83	26.93	32.23	32.97	elaine.512	30.34	30.93	35.71	35.67
4.1.08	32.15	32.03	43.26	44.30	7.1.01	30.50	30.50	36.70	37.10	fireworks	39.62	39.52	52.40	53.24
4.2.01	33.89	33.92	40.96	41.02	7.1.02	35.54	35.69	42.31	42.92	flower_foveon	45.28	45.19	52.17	52.87
4.2.02	31.19	31.02	38.68	38.35	7.1.03	30.55	30.58	35.41	36.28	hdr	42.00	42.08	51.27	51.50
4.2.03	21.92	21.84	27.95	27.77	7.1.04	31.20	30.95	36.95	37.48	house	26.79	26.80	35.15	35.13
4.2.04	30.52	30.65	38.64	38.88	7.1.05	27.43	27.47	32.59	32.97	leaves_iso_200	27.53	27.59	36.69	37.24
4.2.05	29.16	29.17	38.28	38.29	7.1.06	27.55	27.59	32.67	33.26	leaves_iso_1600	28.19	28.19	38.61	39.29
4.2.06	26.36	26.42	33.26	34.12	7.1.07	28.54	28.55	33.22	33.96	nights_iso_100	40.20	40.17	50.99	51.13
4.2.07	30.40	30.22	36.92	37.37	7.1.08	32.48	32.58	37.42	38.14	nights_iso_1600	34.43	34.78	39.07	40.81
5.1.09	29.44	29.59	33.73	35.16	7.1.09	28.41	28.44	34.08	34.43	spider_web	45.14	45.13	54.08	54.21
5.1.10	22.43	22.44	28.87	29.39	7.1.10	31.74	31.70	36.92	37.68					
5.1.11	31.65	31.67	42.54	42.53	7.2.01	33.11	33.43	36.92	37.99					

Table 1: Deviation of compressed images to their uncompressed counterparts at bit rates of 0.2 bits per pixel and 1.2 bits per pixel measured by PSNR for hybrid transform coding with standard filters (Std) and optimized filters (Opt).

7. REFERENCES

- [1] L. Jacques, L. Duval, C. Chaux, and G. Peyré, “A panorama on multiscale geometric representations, intertwining spatial, directional and frequency selectivity,” *Signal Process.*, vol. 91, no. 12, pp. 2699–2730, 2011.
- [2] M.N. Do and M. Vetterli, “The contourlet transform: An efficient directional multiresolution image representation,” *IEEE Trans. Image Process.*, vol. 14, no. 12, pp. 2091–2106, 2005.
- [3] N. Riazifar and M. Yazdi, “Effectiveness of contourlet vs wavelet transform on medical image compression: a comparative study,” *World Academy of Science, Engineering and Technology*, vol. 25, pp. 873–842, 2009.
- [4] T. Peipei and Z. Wei, “Image coding based on sparsified contourlet and adjusted spht,” in *Int. Conf. on Signal Process.*, 2012, pp. 922–925.
- [5] V. Chappelier, C. Guillemot, and S. Marinković, “Image coding with iterated contourlet and wavelet transforms,” in *Int. Conf. on Image Process.*, 2004, pp. 3157–3160.
- [6] S. Phoong, C.W. Kim, P.P. Vaidyanathan, and R. Ansari, “A new class of two-channel biorthogonal filter banks and wavelet bases,” *IEEE Trans. Signal Process.*, vol. 43, no. 3, pp. 649–665, 1995.
- [7] A. Cohen, I. Daubechies, and J.-C. Feauveau, “Biorthogonal bases of compactly supported wavelets,” *Communications on Pure and Applied Mathematics*, vol. 45, no. 5, pp. 485–560, 1992.
- [8] G. Yang, X. Fang, M. Jing, S. Zhang, and M. Hou, “Contourlet filter design based on Chebyshev best uniform approximation,” *EURASIP Journal on Advances in Signal Process.*, vol. 2010, no. 398385, 2010.
- [9] A.L. da Cunha and M.N. Do, “On two-channel filter banks with directional vanishing moments,” *IEEE Trans. Image Process.*, vol. 16, no. 5, pp. 1207–1219, 2007.
- [10] M.D. Adams and D. Xu, “Optimal design of high-performance separable wavelet filter banks for image coding,” *Signal Process.*, vol. 90, no. 1, pp. 180–196, 2010.
- [11] Y. Chen, M.D. Adams, and W. Lu, “Design of optimal quincunx filter banks for image coding,” *EURASIP Journal on Advances in Signal Process.*, vol. 2007, no. 83858, 2007.
- [12] T. Gehrke, T. Greiner, and W. Rosenstiel, “Image content matched directional filters for image coding based on contourlet transform,” in *IEEE Picture Coding Symposium*, 2013, pp. 237–240.
- [13] I. Daubechies and W. Sweldens, “Factoring wavelet transforms into lifting steps,” *Journal of Fourier Analysis and Applications*, vol. 4, no. 3, pp. 247–269, 1998.
- [14] N.S. Jayant and P. Noll, *Digital Coding of Waveforms: Principles and Applications to Speech and Video*, Prentice-Hall, Englewood Cliffs, 1984.
- [15] J. Katto and Y. Yasuda, “Performance evaluation of subband coding and optimization of its filter coefficients,” *Journal of Visual Communication and Image Representation*, vol. 2, no. 4, pp. 303–313, 1991.